Black soliton in a quasi-one-dimensional trapped fermion-fermion mixture

Sadhan K. Adhikari*

Instituto de Física Teórica, UNESP − São Paulo State University, 01.405-900 São Paulo, São Paulo, Brazil
(Dated: February 6, 2008)

Employing a time-dependent mean-field-hydrodynamic model we study the generation of black solitons in a degenerate fermion-fermion mixture in a cigar-shaped geometry using variational and numerical solutions. The black soliton is found to be the first stationary vibrational excitation of the system and is considered to be a nonlinear continuation of the vibrational excitation of the harmonic oscillator state. We illustrate the stationary nature of the black soliton, by studying different perturbations on it after its formation.

I. INTRODUCTION

The one-dimensional nonlinear Schrödinger (NLS) equation in the repulsive or self-defocusing case is usually written as [1]

$$iu_t + u_{xx} - |u|^2 u = 0, \qquad (1.1)$$

where the time (t) and space (x) dependences of the wave function $u(x, t)$ are suppressed. This equation sustains the following dark and grey solitons [2]:

$$u(x, t) = r(x - ct) \exp[-i\{\phi(x - ct) - \mu t\}], \quad (1.2)$$

with

$$r^2(x - ct) = \eta - 2\xi^2 \mathrm{sech}^2[\xi(x - ct)], \qquad (1.3)$$
$$\phi(x - ct) = \tan^{-1}[-2\xi/c \tanh\{\xi(x - ct)\}], \ (1.4)$$
$$\xi = \sqrt{(2\eta - c^2)/2}, \qquad (1.5)$$

where c is the velocity, μ is the chemical potential, and η is related to intensity. Soliton (1.2) having a "notch" over a background density is grey in general. It is dark if density $|u|^2 = 0$ at the minimum. At zero velocity the soliton becomes a stationary dark soliton or a black soliton: $|u(x, t)| = \sqrt{\eta} \tanh[x\sqrt{\eta/2}]$.

The similarity of the NLS equation (1.1) to the mean-field Gross-Pitaevskii (GP) equation describing a trapped zero-temperature Bose-Einstein condensate (BEC) [3] imply the possibility of a stationary dark soliton, or a black soliton, in a trapped BEC or in a degenerate trapped boson-fermion mixture (DBFM) [4]. Dark solitons represent a local minimum in a trapped BEC and have been the topic of both experimental [5] and theoretical [4, 6, 7] investigations. Both DBFM [8] and degenerate fermion-fermion mixture (DFFM) [9] have been experimentally observed and studied theoretically [10, 11]. It has been suggested that the black soliton of a harmonically trapped BEC could be a stationary eigenstate [4]

of the GP equation [3] as in the case of the trap-less NLS equation. We demonstrated that the black soliton in a trapped zero-temperature BEC [12] or a DBFM [13] is the first stationary vibrational excitation of the nonlinear dynamical equation for the respective systems. No such vibrational excitation of the NLS equation (1.1) exists in the absence of a harmonic trap.

In this paper we study the numerical simulation of a black or a stationary dark soliton in a trapped DFFM. We use a coupled time-dependent mean-field-hydrodynamic model for a DFFM and consider the formation of black solitons in a quasi-one-dimensional cigar-shaped geometry using numerical and variational solutions. The present model is inspired by the success of a similar model used recently in the investigation of collapse [14], bright [15] and dark [13] solitons in a DBFM and of mixing-demixing in a DFFM [16]. The black soliton of a DFFM is demonstrated to be a stationary vibrational excitation of the mean-field-hydrodynamic model.

We suggest a scheme for numerical simulation of a stationary dark soliton in trapped DFFM by time evolution of the linear harmonic oscillator equation starting with the analytic vibrational excitation, while the nonlinearities corresponding to the mean-field-hydrodynamic equations are slowly introduced. The simulation proceeds through successive eigenstates of the dynamical model. To illustrate the stability of our scheme we study the oscillation of the stationary dark soliton upon application of different perturbations [12].

Collective excitations in the form of solitons and vortices in trapped fermions have also been investigated recently by Damski et al. [17] and Karpiuk et al. [18]. However, these authors considered isolated ultra-cold fermions and not a realistic DFFM as in the experiments and as discussed in this paper. Also they did not demonstrate the existence of stable dark solitons with a zero at the center of the notch as in the present study. They identified grey soliton-like structure with a shallow dip in the isolated fermionic density distribution quite distinct from the stable fermionic dark solitons in a DFFM as noted in this investigation.

Though the present dark solitons are stable in the mean-field formulation, they could be unstable physically due to quantum fluctuations [19]. The effect of quantum

fluctuations is lost in the mean-free model and can only be studied in a field-theoretic approach. Moreover being an excited state they are thermodynamically unstable. There have been suggestions about how to excite a dark soliton by phase imprinting method [17, 18]. The dark soliton is the lowest vibrational excitation of the mean-field model [12] and there have also been investigations about how to attain such excited states [20]. Nevertheless, despite different suggestions about how to excite a dark soliton [17, 18, 20], experiments to date have not yet generated a stationary dark soliton. Experimentally, so far the dark solitons have been unstable [4]. However, considering that they are stationary excitations of the mean-field-hydrodynamic equation their creation *must* be possible at least as a non-stationary dark soliton which may turn grey and oscillate before decaying due to quantum fluctuations and thermodynamic effects.

The plan of the paper is as follows. In Sec. II we present the mean-field-hydrodynamic model which we use in the present study. We also perform a reduction of the model equations to a quasi-one-dimensional form in a cigar-shaped geometry. In Sec. III we present a variational analysis of the mean-field equations. In Sec. IV we present the numerical results for stationary dark solitons and compare with the variational results. The stationary nature of the dark solitons is illustrated through a numerical study of their dynamics under different perturbing forces. Finally, we present a summary in Sec. V.

II. MEAN-FIELD-HYDRODYNAMIC MODEL

To develop a set of practical time-dependent mean-field-hydrodynamic equations for a DFFM, we consider the following Lagrangian density [13, 15]

$$\mathcal{L} = \frac{i}{2}\hbar \sum_{j=1}^{2} \left(\Psi_j \frac{\partial \Psi_j^{*}}{\partial t} - \Psi_j^{*} \frac{\partial \Psi_j}{\partial t} \right) + g_{12} n_1 n_2$$
$$+ \sum_{j=1}^{2} \left(\frac{\hbar^2 |\nabla \Psi_j|^2}{6m_j} + V_j n_j + \frac{3}{5} A_j n_j^{5/3} \right), \qquad (2.1)$$

where m_j is the mass of component $j(=1,2)$, Ψ_j a complex probability amplitude, $n_j = |\Psi_j|^2$ the real probability density, $N_j \equiv \int d\mathbf{r} n_j(\mathbf{r})$ the number of respective atoms, $A_j = \hbar^2 (6\pi^2)^{2/3}/(2m_j)$, and V_j is the confining trap. Here the interspecies coupling is $g_{12} = 2\pi\hbar^2 a_{12}/m_R$ with the reduced mass $m_R = m_1 m_2/(m_1 + m_2)$, and a_{12} is the interspecies scattering length. The interaction between intra-species fermions in spin-polarized state is highly suppressed due to the Pauli blocking term $3A_j n_j^{5/3}/5$ and has been neglected in Eq. (2.1) and will be neglected throughout. The kinetic energy terms in this equation $\hbar^2 |\nabla \Psi_j|^2/(6m_j)$ are derived from a hydrodynamic equation for the fermions [11] and contribute little to this problem compared to the dominating Pauli

blocking term in Eq. (2.1). However, the inclusion of the kinetic energy terms in Eq. (2.1) leads to a smooth solution for the probability density everywhere [15]. To keep the algebra simple and without losing generality, in our calculation we shall take equal fermion masses: $m_1 = m_2 \equiv m/3$. This simulates well the fermion mixtures in two hyperfine states of ^{6}Li and ^{40}K atoms observed experimentally [9]. The Lagrangian density of each fermion component in Eq. (2.1) is identical to that used in Refs. [13, 15].

The mean-field dynamical equations for the system are just the usual Euler-Lagrange (EL) equations [21]

$$\frac{d}{dt} \frac{\partial \mathcal{L}}{\partial \frac{\partial \Psi_j^*}{\partial t}} + \sum_{k=1}^{3} \frac{d}{dx_k} \frac{\partial \mathcal{L}}{\partial \frac{\partial \Psi_j^*}{\partial x_k}} = \frac{\partial \mathcal{L}}{\partial \Psi_j^*}, \qquad (2.2)$$

where $x_k, k = 1, 2, 3$, are the three space components. With Lagrangian density (2.1) the following EL equations of motion are derived in a straight-forward fashion [14, 15]:

$$\left[-i\hbar \frac{\partial}{\partial t} - \frac{\hbar^2 \nabla_{\mathbf{r}}^2}{6m_j} + V_j(\mathbf{r}) + A_j n_j^{2/3} + g_{12} n_k \right] \Psi_j = 0,$$
$$j \neq k = 1, 2. \qquad (2.3)$$

This is essentially a time-dependent version of a similar time-independent model used recently for fermions [22]. For a stationary state Eqs. (2.3) yield the same result as the formulation of Ref. [11, 22]. For a system with large number of fermions both reduce to [14, 22] the well-known Thomas-Fermi approximation [3, 23]: $n_j = [(\mu_j - V_j)/A_j]^{3/2}$, with μ_j the chemical potential.

We reduce Eq. (2.3) to a minimal quasi-one-dimensional form in a cigar-shaped geometry where the confining trap of anisotropy ν has the form $V_j(\mathbf{r}) = \frac{1}{2}3m_j\omega^2(\rho^2 + \nu^2 z^2)$, with ρ the radial vector and z the axial vector. For a cigar-shaped geometry $\nu << 1$, we consider solutions of Eq. (2.3) of the type $\Psi_j(\mathbf{r}, t) = \sqrt{N_j}\phi_j(x,\tau)\psi_j^{(0)}(\rho)/\sqrt{l}$, where $x = z/l$, $\tau = t\nu\omega/2$, $l = \sqrt{\hbar/(\nu\omega m)}$ and $\psi_j^{(0)}(\rho)$ is the circularly symmetric ground-state linear harmonic-oscillator wave function. In the $\nu << 1$ limit the quasi-one-dimensional functions $\phi_j(x,\tau)$ satisfy the following dimensionless equations [16]:

$$\left[-i\frac{\partial}{\partial \tau} - \frac{\partial^2}{\partial x^2} + x^2 + \mathcal{N}_{jk} |\phi_k|^2 \right.$$
$$\left. + \mathcal{N}_{jj} |\phi_j|^{4/3} \right] \phi_j(x,\tau) = 0, \quad j \neq k = 1, 2, \quad (2.4)$$

where $\mathcal{N}_{jk} = 12a_{12}(N_k/\nu)/l$, and $\mathcal{N}_{jj} = 9(6\pi N_j/\nu)^{2/3}/5$. In Eq. (2.4), the normalization condition is given by $\int_{-\infty}^{\infty} |\phi_j(x,\tau)|^2 dx = 1$.

In case when $N_1 = N_2 = N$, the two equations (2.4) become identical and reduce to

$$\left[-i\frac{\partial}{\partial \tau} - \frac{\partial^2}{\partial x^2} + x^2 + \gamma |\phi|^2 + \beta |\phi|^{4/3} \right] \phi(x,\tau) = 0,$$
$$(2.5)$$

which permits the solution $\phi = \phi_1 = \phi_2$, with $\beta = \mathcal{N}_{jj}$ and $\gamma = \mathcal{N}_{jk}$.

III.   VARIATIONAL ANALYSIS

A.   Symmetric Case ($N_1 = N_2$)

Next we present a variational analysis of Eq. (2.5) based on the stationary trial wave function [24]

$$\phi_v(x,\tau) = A(\tau)x \exp\left[-\frac{x^2}{2R^2(\tau)} + \frac{i}{2}b(\tau)x^2 + ic(\tau)\right], \tag{3.1}$$

where A is the amplitude, R is the width, b the chirp, and c the phase. The Lagrangian density for Eq. (2.5) is the one-term version of Eq. (2.1), e.g.,

$$\mathcal{L} = \frac{i\hbar}{2}\left[\phi_v \frac{\partial \phi_v^*}{\partial t} - \phi_v^* \frac{\partial \phi_v}{\partial t}\right] + \left|\frac{\partial \phi_v}{\partial x}\right|^2 + \frac{1}{2}\gamma n^2 + \frac{3}{5}\beta n^{5/3}$$
$$+ \ x^2 n \tag{3.2}$$

which is evaluated with this trial function and the effective Lagrangian $L = \int_{-\infty}^{\infty} \mathcal{L}(\varphi_v)dx$ becomes

$$L = \frac{A^2 R^3 \sqrt{\pi}}{2}\left(\alpha\beta(AR)^{4/3} + \dot{c} + \frac{3R^2\dot{b}}{4} + \frac{3\gamma}{16\sqrt{2}}A^2 R^2\right.$$
$$+ \ \frac{3}{2R^2} + \frac{3}{2}b^2 R^2 + \frac{3}{2}R^2\bigg), \tag{3.3}$$

where $\alpha = (54/125\sqrt{\pi})(3/5)^{1/6}\Gamma(13/6) \approx 0.242269$ and the overhead dot denotes time derivative. The variational Lagrange equations [21]

$$\frac{d}{dt}\frac{\partial L}{\partial \dot{q}} = \frac{\partial L}{\partial q}, \tag{3.4}$$

where q stands for c, A, R and b can then be written as

$$\frac{\sqrt{\pi}}{2}A^2 R^3 = \text{constant} = 1. \tag{3.5}$$

$$3\dot{b} = -\frac{6}{R^4} - 6b^2 - \frac{3\gamma A^2}{2\sqrt{2}} - 6 - \frac{20}{3}\alpha\beta\frac{A^{4/3}}{R^{2/3}} - \frac{4\dot{c}}{R^2}(3.6)$$

$$5\dot{b} = -\frac{2}{R^4} - 10b^2 - \frac{5\gamma A^2}{4\sqrt{2}} - 10 - \frac{52}{9}\alpha\beta\frac{A^{4/3}}{R^{2/3}} - \frac{4\dot{c}}{R^2}, \tag{3.7}$$

$$\dot{R} = 2Rb. \tag{3.8}$$

The constant in Eq. (3.5) is fixed by the normalization condition. Eliminating $\dot{c}$ from Eqs. (3.6) and (3.7) we obtain

$$2\dot{b} = \frac{4}{R^4} - 4b^2 + \gamma\frac{A^2}{4\sqrt{2}} - 4 + \frac{8}{9}\alpha\beta\frac{A^{4/3}}{R^{2/3}}. \tag{3.9}$$

The use of Eqs. (3.5), (3.8) and (3.9) leads to the following differential equation for the width R:

$$\frac{d^2R}{d\tau^2} = \left(\frac{4}{R^3} + \frac{\gamma}{2\sqrt{2\pi}R^2} - 4R + \frac{8}{R^{5/3}}\frac{2^{2/3}\alpha\beta}{9\pi^{1/3}}\right), \tag{3.10}$$

$$= -\frac{d}{dR}\left[\frac{2}{R^2} + \frac{\gamma}{R}\frac{1}{2\sqrt{2\pi}} + 2R^2 + \frac{4\alpha\beta}{3}\left(\frac{4}{\pi R^2}\right)^{1/3}\right]. \tag{3.11}$$

The quantity in the square bracket is the effective potential of the equation of motion. Small oscillation around a stable configuration is possible when there is a minimum in this potential. The variational result for width R follows by setting the right-hand-side of Eq. (3.10) to zero corresponding to a minimum in this effective potential, from which the variational profile for the soliton can be obtained [24] using Eq. (3.1).

B.   Asymmetric Case ($N_1 \neq N_2$)

The above variational analysis can be extended to the asymmetric case. However, the algebra becomes quite involved if we take a general variational trial wave function with chirp and phase parameters. As we are interested mostly in the density profiles, we consider the following normalized stationary trial wave function for fermion component j of Eq. (2.4)

$$\varphi_{vj} = \sqrt{\frac{2}{R_j^3(\tau)\sqrt{\pi}}}x \exp\left[-\frac{x^2}{2R_j^2(\tau)}\right], \quad j = 1, 2. \tag{3.12}$$

Using essentially the Lagrangian density (2.1) in this case we obtain the following effective Lagrangian

$$L = \frac{3N_{jk}}{\sqrt{\pi}}\frac{R_1^2 R_2^2}{(R_1^2 + R_2^2)^{5/2}} + \sum_{j=1}^{2}\left(\frac{\alpha 2^{2/3}}{\pi^{1/3}}\frac{N_{jj}}{R_j^{2/3}} + \frac{3(R_j^4 + 1)}{2R_j^2}\right). \tag{3.13}$$

The variational Lagrange equations (3.4) for R_1 and R_2 now become

$$\frac{4}{R_j^3} - 4R_j - \frac{4N_{jk}}{\sqrt{\pi}}\frac{2R_j R_k^4 - 3R_j^3 R_k^2}{(R_1^2 + R_2^2)^{7/2}} + \frac{2^{2/3}}{9\pi^{1/3}}\frac{8\alpha N_{jj}}{R_j^{5/3}} = 0. \tag{3.14}$$

Equations (3.14) can be solved for the variational widths R_j and consequently the variational profile of the wave functions obtained from Eq. (3.12). When $N_1 = N_2$, in Eq. (3.14) $N_{jj} = \beta$, $N_{jk} = N_{kj} = \gamma$ and $R_1 = R_2 = R$; and in this case it is verified that Eq. (3.14) yields the same variational widths as from the result obtained in the symmetric case in Sec. IIIA given by Eq. (3.10); e. g.,

$$\frac{4}{R^3} - 4R + \frac{\gamma}{R^2}\frac{1}{2\sqrt{2\pi}} + \frac{2^{2/3}}{R^{5/3}}\frac{8\beta\alpha}{9\pi^{1/3}} = 0. \tag{3.15}$$
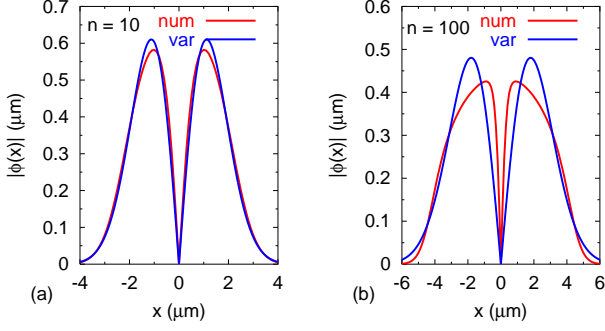
FIG. 1: (Color online) The solitons $|\phi(x)|$ of BEC from the numerical solution of Eq. (3.16) (denoted num) vs. x for (a) $n = 10$ and (b) $n = 100$. The corresponding variational solutions obtained from Eq. (3.17) (denoted var) are also shown.

FIG. 2: (Color online) The black soliton $|\phi(x)|$ from the numerical solution of Eq. (2.5) (denoted num) vs. x for a DFFM with $N_1 = 10$, $N_2 = 10$, $a_{12}/l = 0.05$, while $N_{11} = N_{22} \approx 275$, and $N_{ij} = 60$. The corresponding variational solution obtained from Eq. (3.17) (denoted var) is also shown.

C. Black Soliton in a BEC

By a variational calculation we establish the stability of a black soliton in a trapped BEC satisfying the one-dimensional GP equation:

$$\left[-i\frac{\partial}{\partial \tau} - \frac{\partial^2}{\partial x^2} + x^2 + n\,|\phi|^2 \right] \phi(x, \tau) = 0. \qquad (3.16)$$

This equation is identical with Eq. (2.5) with $\beta = 0$ and $\gamma = n$. Hence the variational analysis of Sec. IIIA applies to this case and the differential equation for width R is given by Eq. (3.10) with $\beta = 0$:

$$\frac{d^2 R}{d\tau^2} = \left(\frac{4}{R^3} + \frac{n}{2\sqrt{2\pi}R^2} - 4R \right). \qquad (3.17)$$

The variational width in this case is given by setting the right-hand-side of this equation to zero.

IV. NUMERICAL RESULTS

We solve Eqs. (2.4) for bright solitons numerically using a time-iteration method based on the Crank-Nicholson discretization scheme elaborated in Ref. [25]. We discretize the coupled partial differential equations (2.4) using time step 0.0004 and space step 0.02 in the domain $-16 < x < 16$. The second derivative in x is discretized by a three-point finite-difference rule and the first derivative in time by a two-point finite-difference rule. We start a time evolution of Eqs. (2.4) setting the nonlinear terms to zero, and starting with the eigenfunction of the linear harmonic oscillator problem: $\phi(x, \tau) = \sqrt{(2/\sqrt{\pi})}x \exp(-x^2/2) \exp(-3i\tau)$. During the time evolution the nonlinear terms are switched on slowly and the time evolution continued to obtain the final converged solutions. In addition to solving the coupled equations (2.4), we also solved the single equation (2.5) in the symmetric case: $N_1 = N_2$ and Eq. (3.16) for bosons.
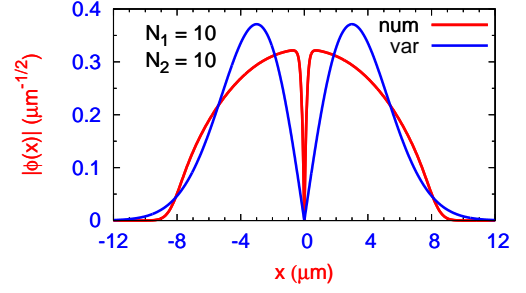
In our numerical study we take $l = 1$ μm and consider a DFFM consisting of two electronic states of ^{40}K atoms. For a BEC we consider ^{39}K atoms. This corresponds to a radial trap of frequency $\omega = \hbar/(l^2 m) \approx 500$ Hz. Consequently, the unit of time is $2/\omega \approx 4$ ms. For another fermionic atom the ω value gets changed accordingly for $l = 1$ μm.

A. Black Soliton in a BEC

The results for black solitons in a BEC are obtained by solving Eqs. (3.16) and (3.17) and are presented in Figs. 1 (a) and (b) for $n = 10$ and 100, respectively, where the soliton profiles are displayed. The variational profiles lie close to the numerical results and confirm the existence of a black soliton in this case. For smaller values of nonlinearity, the solitons have a probability distribution close to the ansatz given by (3.1). Consequently, the variational result is more accurate. For larger nonlinearities the actual probability distribution obtained from the numerical solution deviates from ansatz (3.1) as can be seen from Fig. 1 (b). By construction the variational ansatz (3.1) is stationary. The close agreement between the variational and numerical solutions demonstrates the stationary nature of these dark solitons. Hence, contrary to comments in the literature [7], these black solitons of a trapped BEC are stationary. Although, we illustrate the present simulation for a black soliton for a repulsive BEC, stationary dark soliton also exists for an attractive BEC [12].

B. Black Soliton in a DFFM

The numerical results for black solitons in a DFFM are obtained by solving Eqs. (2.5) and (2.4) for the symmetric ($N_1 = N_2$) and asymmetric ($N_1 \neq N_2$) cases, respectively. The corresponding variational results are obtained from Eqs. (3.15) and (3.14), respectively. First
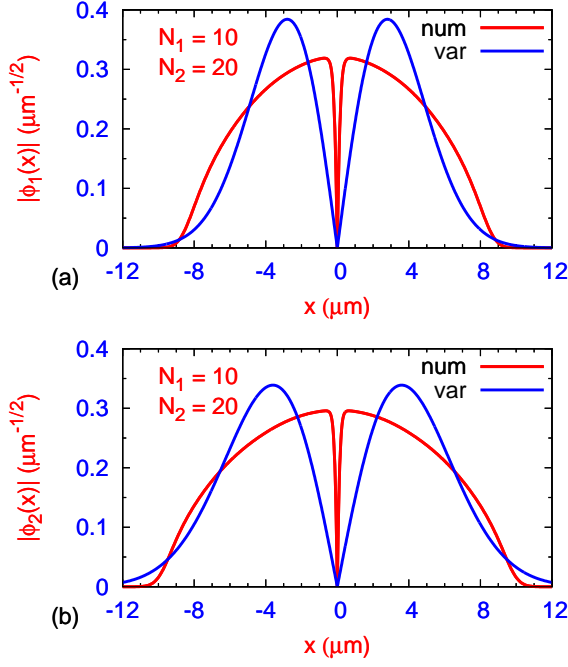
(a)

(b)

FIG. 3: (Color online) The black solitons (a) $\phi_1(x)$ and (b) $\phi_2(x)$ from the numerical solution of Eqs. (2.4) (denoted num) for a DFFM with $N_1 = 10$, $N_2 = 20$, $a_{12}/l = 0.05$, while $\mathcal{N}_{11} \approx 275$, $\mathcal{N}_{22} \approx 436$, $\mathcal{N}_{12} = 120$, and $\mathcal{N}_{21} = 60$. The corresponding variational solutions (denoted var) obtained from Eqs. (3.14) are also shown.

we present the numerical and variational results for the symmetric situation with $a_{12}/l = 0.05$, $\nu = 0.1$, and $N_1 = N_2 = 10$ in Fig. 2. The nonlinearities here are quite large, e.g., $N_{jj} \approx 275$ and $N_{jk} = 60$, $j \neq k = 1, 2$. The variational and numerical results in this case compare favorably as can be seen in Fig. 2.

Next we present the numerical and variational results for the asymmetric case with $N_1 = 10$ and $N_2 = 20$. $a_{12}/l = 0.05$, and $\nu = 0.1$ corresponding to even larger nonlinearities $\mathcal{N}_{11} \approx 275$, $\mathcal{N}_{22} \approx 436$, $\mathcal{N}_{12} = 120$, and $\mathcal{N}_{21} = 60$. The variational and numerical results in this case for black solitons for components 1 and 2 are exhibited in Fig. 3 (a) and (b).

From Figs. 1−3 we see that although the variational result is a good quantitative approximation to the exact result for small values of nonlinearity (Figs. 1), it ceases to be so for larger values of nonlinearity (Figs. 2 and 3). This is true, as for large values of nonlinearity the harmonic-oscillator ansatz for the soliton profile (3.1) is not a good approximation to the accurate numerical result. In other words, the variational calculation confirms a stationary black soliton in all cases. A poor initial variational harmonic-oscillator ansatz for the soliton is responsible for the imprecise variational results for large nonlinearities.

To demonstrate the robustness of the black solitons, we introduced a displacement in the notch of the black
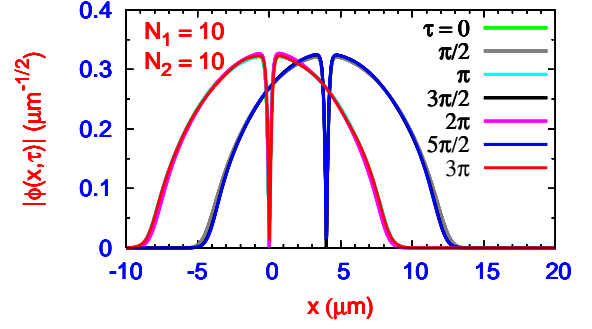

FIG. 4: (Color online) The dark soliton profile for the black soliton of a DFFM of Fig. 2 with $N_1 = N_2 = 10$ at times $\tau = 0, \pi/2, \pi, 3\pi/2, 2\pi, 5\pi/2$, and 3π after the soliton has been set into oscillation by displacing the trap through a distance of 2 μm.
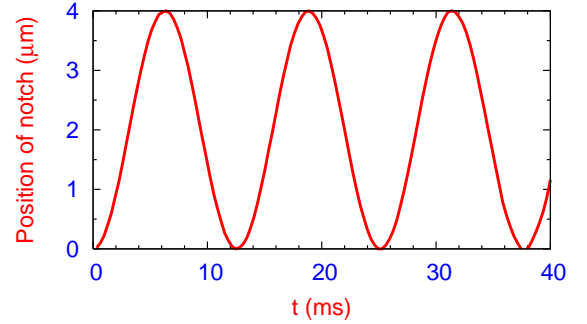

FIG. 5: (Color online) The simple harmonic motion of the minimum of the notch of the black soliton(s) of Fig. 2 after the soliton(s) have been set into oscillation by displacing the trap through a distance of 2 μm.

soliton upon formation by displacing the center of the harmonic trap by a small distance. The dark soliton(s) execute harmonic oscillation for small displacements during a moderate time interval. For the soliton of Fig. 2 with $N_1 = N_2 = 10$ the oscillation is illustrated in Fig. 4 by exhibiting successive snapshots of the dark soliton at positions of maximum displacement at times $\tau = 0, \pi/2, \pi, 3\pi/2, 2\pi, 5\pi/2$ and 3π for a trap displacement of 2 μm at time 0. The soliton remains black at all times with the minimum at the notch equaling zero. The simple harmonic motion of the position of the notch is illustrated in Fig. 5. The angular frequency of oscillation as obtained from Fig. 5 is the trap frequency 500 Hz. The numerical simulations presented in Figs. 4 and 5 demonstrate the stationary nature of the black solitons under small oscillations.

To further demonstrate the stationary nature of the black solitons, after their formation we increased suddenly the strength of the harmonic trap by 10%: $x^2 \rightarrow 1.1x^2$. The stability of the dark soliton for $N_1 = N_2 = 10$ under this sudden change in the trap frequency is exhib-
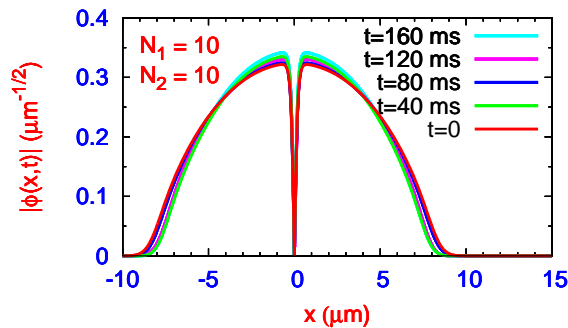
FIG. 6: (Color online) The dark soliton profile for the black soliton of Fig. 2 with $N_1 = N_2 = 10$ at times $t = 0$, 40 ms, 80 ms, 120 ms, and 160 ms after the soliton has been set into breathing oscillation by increasing the strength of the trap by 10%.

ited in Fig. 6 where we plot the soliton profile at different times. The soliton executes reasonably stable breathing oscillation. To study the breathing oscillation in detail we calculate the root-mean-square (rms) size $\langle s \rangle$ of the soliton at different times from a numerical solution of the mean-field equation and the result is plotted in Fig. 7 (a). We also solved the variational equation (3.10), an ordinary differential equation by a fourth-order Runge-Kutta rule, to calculate the size of the soliton and the time variation of the results is plotted in Fig. 7 (b). The amplitude and frequency of the variational oscillation are in good qualitative agreement with the precise numerical results. However, there is quantitative disagreement between the two. After multiplying the variational size by 0.89, the results in Fig. 7 (b) are in good agreement with the numerical result in Fig. 7 (a). The period of breathing oscillation from Fig. 7 (a) is 7.3 ms and that from Fig. 7 (b) is 7.6 ms. The fair agreement between the variational and numerical results of breathing oscillation illustrates that the variational description of the stationary dark soliton is on the right track and confirms the stationary nature of the black soliton.

V. SUMMARY

In conclusion, we used a coupled mean-field-hydrodynamic model for a DFFM to study the formation of black solitons in a quasi-one-dimensional geometry by

numerical and variational methods. The existence of stationary dark solitons is predicted by variational study and confirmed by detailed numerical analysis. The stationary nature of the present solitons is demonstrated numerically through their (a) sustained oscillation initiated by a sudden displacement of the harmonic trap, as well as (b) breathing oscillation initiated by a sudden increase of the strength of the harmonic trap by 10%: $x^2 \to 1.1x^2$. Here we used a set of mean-field equations for the DFFM. A proper treatment of a degenerate Fermi gas or DFFM
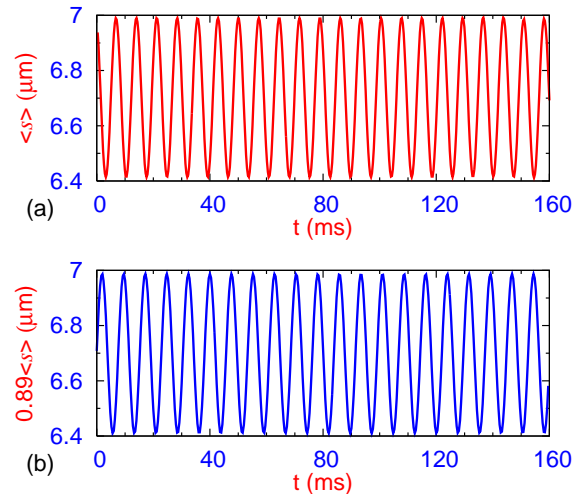

FIG. 7: (Color online) The periodic motion of the rms size $\langle s \rangle$ of the dark soliton after suddenly increasing the strength of the trap by 10 %: (a) numerical result, (b) variational result.

should be done using a fully antisymmetrized many-body Slater determinant wave function [10] as in the case of scattering involving many electrons [26]. However, in view of the success of a fermionic mean-field model in studies of collapse [14], bright [15] and dark [13] soliton in a DBFM and of mixing and demixing in a DFFM [16], we do not believe that the present study on bright solitons in a DFFM to be so peculiar as to have no general validity.

[1] Y. S. Kivshar and G. P. Agrawal, *Optical Solitons - From Fibers to Photonic Crystals* (Academic, San Diego, 2003).

[2] P. G. Drazin, R. S. Johnson, *Solitons: An Introduction,* (Cambridge University Press, Cambridge, 1989).

[3] F. Dalfovo, S. Giorgini, L. P. Pitaevskii, and S. Stringari, Rev. Mod. Phys. **71**, 463 (1999); V. I. Yukalov, Laser

Phys. Lett. **1**, 435 (2004); V. I. Yukalov and M. D. Girardeau, Laser Phys. Lett. **2**, 375 (2005).

[4] S. A. Morgan, R. J. Ballagh, and K. Burnett, Phys. Rev. A **55**, 4338 (1997); T. Busch and J. R. Anglin, Phys. Rev. Lett. **84**, 2298 (2000)

[5] J. Denschlag *et al.*, Science **287**, 97 (2000); B. P. Ander-

son *et al.*, Phys. Rev. Lett. **86**, 2926 (2001); S. Burger *et al.*, Phys. Rev. Lett. **83**, 5198 (1999); S. Stock, B. Battelier, V. Bretin, Z. Hadzibabic, and J. Dalibard, Laser Phys. Lett. **2**, 275 (2005).

[6] R. D'Agosta, B. A. Malomed, and C. Presilla, Phys. Lett. A **275**, 424 (2000); N. G. Parker, N. P. Proukakis, C. F. Barenghi, and C. S. Adams, J. Phys. B **37**, S175 (2004); N. P. Proukakis, N. G. Parker, D. J. Frantzeskakis, C. S. Adams, J. Opt. B **6**, S380 (2004); P. J. Y. Louis, E. A. Ostrovskaya, Y. S. Kivshar, J. Opt. B **6**, S309 (2004); V. A. Brazhnyi, V. V. Konotop, Phys. Rev. A **68**, 043613 (2003).

[7] P. G. Kevrekidis, R. Carretero-González, G. Theocharis, D. J. Frantzeskakis, and B. A. Malomed, Phys. Rev. A **68**, 035602 (2003).

[8] F. Schreck *et al.*, Phys. Rev. Lett. **87**, 080403 (2001); A. G. Truscott *et al.*, Science **291**, 2570 (2001); Z. Hadzibabic *et al.*, Phys. Rev. Lett. **88**, 160401 (2002); G. Modugno *et al.*, Science **297**, 2240 (2002); C. Ospelkaus, S. Ospelkaus, K. Sengstock, and K. Bongs, Phys. Rev. Lett. **96**, 020401 (2006).

[9] B. DeMarco and D. S. Jin, Science **285**, 1703 (1999); K. M. O'Hara *et al.*, Science **298**, 2179 (2002).

[10] K. Molmer, Phys. Rev. Lett. **80**, 1804 (1998); R. Roth, Phys. Rev. A **66**, 013614 (2002); T. Miyakawa, T. Suzuki, and H. Yabu, *ibid.* **64**, 033611 (2001); X.-J. Liu, M. Modugno, and H. Hu, *ibid.* **68**, 053605 (2003); X.-J. Liu and H. Hu, *ibid.* **67**, 023613 (2003); M. Modugno *et al.*, *ibid* **68**, 043626 (2003); D. M. Jezek, M. Barranco, M. Guilleumas, R. Mayol, and M. Pi, *ibid* **70**, 043630 (2004).

[11] P. Capuzzi, A. Minguzzi, and M. P. Tosi, Phys. Rev. A **69**, 053615 (2004).

[12] S. K. Adhikari, J. Low Temp. Phys. (in press), cond-mat/0510526.

[13] S. K. Adhikari, J. Phys. B **38**, 3607 (2005).

[14] S. K. Adhikari, Phys. Rev. A **70**, 043617 (2004).

[15] S. K. Adhikari, Phys. Rev. A **72**, 053608 (2005); S.K. Adhikari, Laser Phys. Lett. DOI 10.1002/lapl.200400047.

[16] S. K. Adhikari, Phys. Rev. A **73**, 043619 (2006).

[17] B. Damski, K. Sacha, and J. Zakrzewski, J. Phys. B **35**, L153 (2002).

[18] T. Karpiuk, M. Brewczyk, and K. Rzążewski, J. Phys. B **35**, L315 (2002); E. Witkowska and M. Brewczyk, Phys. Rev. A **72**, 023606 (2005).

[19] J. Dziarmaga, Phys. Rev. A **70**, 063616 (2004); J. Phys. B **36**, 1217 (2003).

[20] V. I. Yukalov, E. P. Yukalova, and V. S. Bagnato, Phys. Rev. A **56**, 4845 (1997); V. I. Yukalov, K. P. Marzlin, and E. P. Yukalova, Phys. Rev. A **69**, 023620 (2004).

[21] H. Goldstein, *Classical Mechanics, 2nd Edition*, (Addison Wesley, Reading, 1980).

[22] Z. Akdeniz, A. Minguzzi, P. Vignolo, and M.P. Tosi, Phys. Lett. A **331**, 258 (2004); P. Capuzzi, A. Minguzzi, and M. P. Tosi, Phys. Rev. A **68**, 033605 (2003).

[23] L. Vichi and S. Stringari, Phys. Rev. A **60**, 4734 (1999).

[24] D. Anderson, Phys. Rev. A **27**, 3135 (1983).

[25] S. K. Adhikari and P. Muruganandam, J. Phys. B **35**, 2831 (2002); P. Muruganandam and S. K. Adhikari, *ibid.* **36**, 2501 (2003).

[26] P. K. Biswas and S. K. Adhikari, J. Phys. B **33**, 1575 (2000); **31**, L737 (1998); **31**, 3147 (1998); **31**, L315 (1998); S. K. Adhikari, Phys. Rev. C **19**, 1729 (1979); L. Tomio and S. K. Adhikari, Phys. Rev. C **22**, 28 (1980).